RESEARCH ARTICLE

Magnetic Resonance in Medicine

Defect distribution index: A novel metric for functional lung MRI in cystic fibrosis

Anne Valk[1,2] 🆔 | Corin Willers[1] 🆔 | Kamal Shahim[1] | Orso Pusterla[1,3,4,5] 🆔 |
Grzegorz Bauman[3,4] 🆔 | Robin Sandkühler[4] | Oliver Bieri[3,4] | Florian Wyler[1] 🆔 |
Philipp Latzin[1] 🆔

[1]Division of Paediatric Respiratory Medicine and Allergology, Department of Paediatrics, Inselspital, Bern University Hospital, University of Bern, Bern, Switzerland

[2]Division of Paediatric Pulmonology and Allergology, Department of Pediatrics, Amalia Children's Hospital, Radboud University Medical Centre, Nijmegen, The Netherlands

[3]Division of Radiological Physics, Department of Radiology, University of Basel Hospital, Basel, Switzerland

[4]Department of Biomedical Engineering, University of Basel, Allschwil, Switzerland

[5]Institute for Biomedical Engineering, University and ETH Zurich, Zurich, Switzerland

Correspondence
Philipp Latzin, Division of Paediatric Respiratory Medicine and Allergology, Department of Paediatrics, Inselspital, Bern University Hospital, University of Bern, Freiburgstrasse 8, 3010 Bern, Switzerland.
Email: philipp.latzin@insel.ch

Purpose: Lung impairment from functional MRI is frequently assessed as defect percentage. The defect distribution, however, is currently not quantified. The purpose of this work was to develop a novel measure that quantifies how clustered or scattered defects in functional lung MRI appear, and to evaluate it in pediatric cystic fibrosis.

Theory: The defect distribution index (DDI) calculates a score for each lung voxel categorized as defected. The index increases according to how densely and how far an expanding circle around a defect voxel contains more than 50% defect voxels.

Methods: Fractional ventilation and perfusion maps of 53 children with cystic fibrosis were previously acquired with matrix pencil decomposition MRI. In this work, the DDI is compared to a visual score of 3 raters who evaluated how clustered the lung defects appear. Further, spearman correlations between DDI and lung function parameters were determined.

Results: The DDI strongly correlates with the visual scoring ($r = 0.90$ for ventilation; $r = 0.88$ for perfusion; $P < .0001$). Although correlations between DDI and defect percentage are moderate to strong ($r = 0.61$ for ventilation; $r = 0.75$ for perfusion; $P < .0001$), the DDI distinguishes between patients with comparable defect percentage.

Conclusion: The DDI is a novel measure for functional lung MRI. It provides complementary information to the defect percentage because the DDI assesses defect distribution rather than defect size. The DDI is applicable to matrix pencil MRI data of cystic fibrosis patients and shows very good agreement with human perception of defect distributions.

1 | INTRODUCTION

Progressive lung disease is the main cause of morbidity and mortality in patients with cystic fibrosis (CF).[1,2] High resolution CT is the current gold standard to assess structural lung damage.[3-5] Although low-dose CT scans are available, the cumulative ionizing radiation risk remains the main drawback of using CT in life-long monitoring of CF patients.[5-8] Sensitive pulmonary function tests, such as the multiple breath washout technique,[9,10] lack precise spatial information.

MRI could serve as a nonionizing radiation alternative to the clinically established imaging modalities. An additional advantage of MRI is the possibility of functional imaging. Ventilation imaging can be obtained with hyperpolarized or fluorinated gas MRI,[11-13] whereas perfusion is routinely assessed using contrast-enhanced MRI techniques.[14] A less invasive alternative for ventilation and perfusion imaging is provided by proton-based functional imaging, for example, using Fourier decomposition[15-18] or matrix pencil decomposition (MP) MRI.[19] No breathing maneuvers, tracer gases, or contrast agents are required.

Current MP MRI outcomes for radiological evaluation are maps of fractional ventilation and perfusion and the derived impaired fractional ventilation and impaired perfusion relative to lung volume, that is, expressed as a defect percentage (DP) (Figure 1).[20] R_{FV} and R_Q are computed from the ventilation and perfusion maps, respectively, by classifying all voxels below a certain threshold of the signal intensity histogram as defect.

Although R_{FV} and R_Q are well suited to monitor CF lung disease,[20,21] they only indicate overall defect percentage. This measure ignores much of the spatial information, specifically the clustering of defect, and therefore does not capture the true potential of lung imaging. To fully understand the course of disease and treatment effects and to improve phenotyping, a comprehensive assessment of existing data is necessary.[22] Two important aspects are currently missing. First, radiologists usually describe spatial location of disease on the basis of anatomical boundaries such as lung lobes. To the best of our knowledge, lobe segmentation is not routinely available for lung MRI.[23] The second missing aspect is the defect distribution, which is described by radiologists as either disseminate and scattered on one hand, or as consolidated and clustered on the other. Describing this distribution of defects with an automatic, comparable method may add valuable clinical information.

Smith et al. reported the number of defects and largest contiguous defect for hyperpolarized gas ventilation MRI in
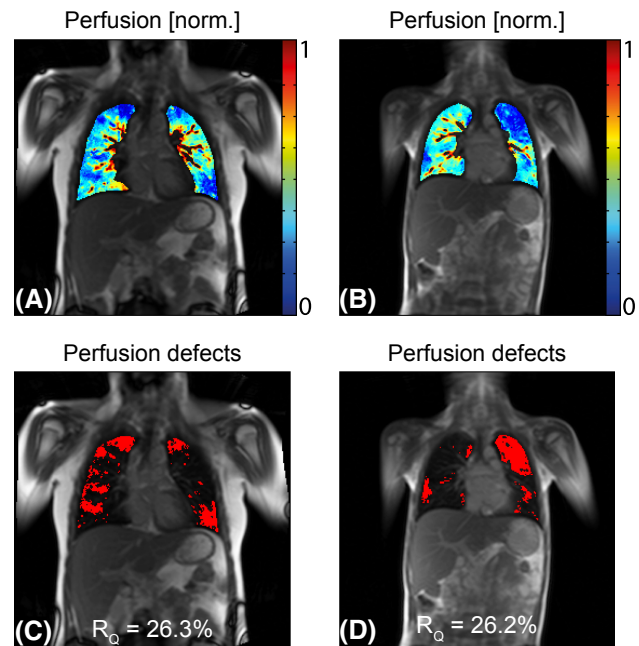
FIGURE 1 Exemplary MP MRI perfusion maps of 2 patients with CF and corresponding perfusion defect map with similar defect percentage but different distribution pattern. (A) and (C) exemplary slice of a 17-year-old girl with R_Q: 26.3% (FEV$_1$: −2.2 z-scores, LCI: 12.8 TO). (B) and (D) exemplary slice of a 7-year-old boy with R_Q: 26.2% (FEV$_1$: −0.9 z-scores, LCI: 8.5 TO). (A) and (B) relative perfusion map, with blue indicating low perfusion. (C) and (D) perfusion defect (red) map with defect percentage. CF, cystic fibrosis; FEV$_1$, forced expiratory volume in 1 s; LCI, lung clearance index; MP, Matrix Pencil decomposition; R_Q, impaired relative perfusion; TO, lung volume turnovers

CF patients,[24] giving an indication of the defect distribution. However, a measure that quantifies clustered defects is currently lacking. This would allow for observer-independent assessment of the defect distribution and would facilitate longitudinal analysis and interindividual comparison. The main purpose of this work was therefore to develop a measure that quantifies clustered defects in functional lung MRI and to apply it to MP MRI defect maps of a pediatric CF population.

2 | THEORY

The defect distribution index (DDI) is applicable to functional lung defect maps (eg, Figure 1C,D). These can be single slices or part of a group of k slices of the same lung. For

explanatory purposes, in this section the DDI is computed on an artificial lung map, sketched in Figure 2A.

For each slice, we have a segmented 2D lung map, containing voxels x_i:

$$seg\left(x_i\right) = \begin{cases} 1: \text{lung tissue} \\ 0: \quad \text{else} \end{cases}$$

Additionally, defect maps distinguish between healthy and defect lung tissue voxels:

$$dm\left(x_i\right) = \begin{cases} 0: \textit{healthy} \\ 1: \textit{defect} \end{cases}$$

We calculate the parameter A_{lung}, which is the mean number of lung tissue voxels across the k slices of the lung under consideration:

$$A_{lung} = \frac{\sum_1^k \sum seg\left(x_i\right)}{k}.$$

This is used as an area normalization. Areas within the lung maps in units of voxels are not inherently meaningful;

however, as a fraction of the above approximation of lung size they allow comparisons between different scales (eg, Supporting Information Figure S1) and resolutions.

A DDI(x_i) is calculated voxelwise for every target defect voxel at position x_i according to the following steps:

1. For a circle centered on the target voxel, with radius r, we can calculate the defect ratio $DR(x_i, r)$. It is computed as the number of defected voxels $D(x_i, r)$ divided by the total number of voxels $A(x_i, r)$, with centers contained within the circle of radius r (Figure 2B,C):

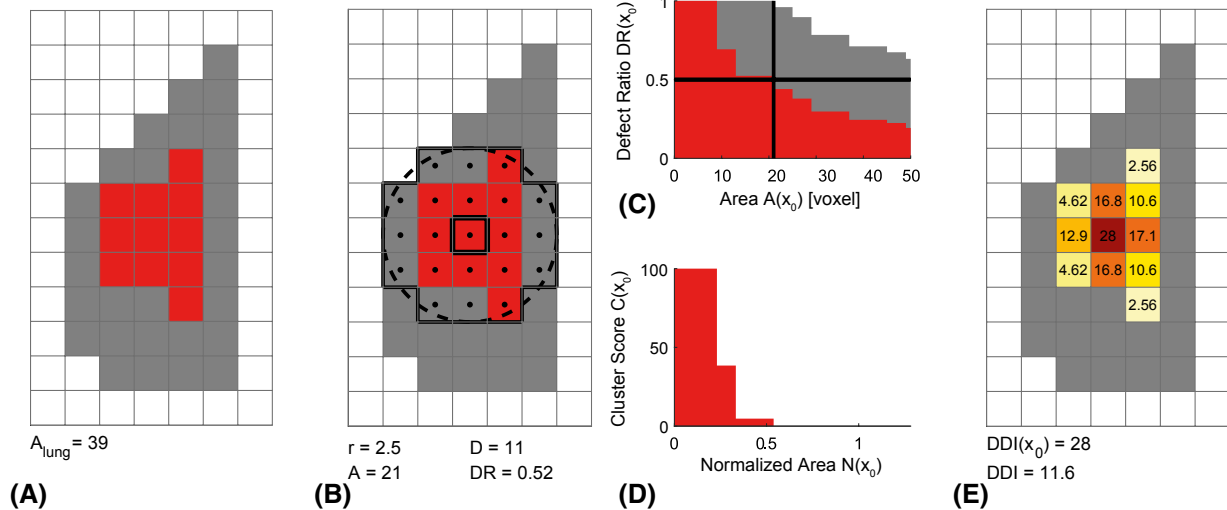$$A\left(x_i, r\right) = \left\{ x_j \big| \left\| x_i - x_j \right\|_2 \le r \right\}$$

$$D\left(x_i, r\right) = \left\{ x_j | dm\left(x_j\right) = 1 \wedge x_j \in A\left(x_i, r\right) \right\}$$

$$DR\left(x_i, r\right) := \frac{\left| D\left(x_i, r\right) \right|}{\left| A\left(x_i, r\right) \right|}.$$

2. From this we calculate the cluster score $C(x_i, r)$, as well as the normalized area $N(x_i, r)$, as a function of r (Figure 2D).

$$C\left(x_i, r\right) := 100 \cdot \frac{DR\left(x_i, r\right) - T}{(1 - T)}$$

(A) $A_{\text{lung}} = 39$

(B) $r = 2.5$ $D = 11$; $A = 21$ $DR = 0.52$

(C) Defect Ratio DR(x_0); Area A(x_0) [voxel]

(D) Cluster Score C(x_0); Normalized Area N(x_0)

(E) 2.56; 4.62 16.8 10.6; 12.9 28 17.1; 4.62 16.8 10.6; 2.56; DDI(x_0) = 28; DDI = 11.6

FIGURE 2 Exemplary DDI calculation. (A) The input for the DDI is a functional lung defect map (eg, Figure 1C,D). Defect voxels are labeled in red, non-defect lung voxels in gray, and non-defect background voxels (regions outside the lung) in white. A $DDI(x_i)$ is calculated for every defect voxel. Note that for simplicity, an artificial lung defect map with a very low number of voxels is displayed here. The reference size of this artificial lung map is 39 voxels. (B) A $DDI(x_i)$ is calculated by centering a circle around the target voxel (x_0, outlined in black) and gradually increasing its radius. An example circle radius r of 2.5 voxel side lengths is displayed (dashed outline). The number of voxels that have their center (marked by dots) inside this radius is 21, so $A(x_0, 2.5) = 21$ voxels. The number of defect voxels among those is $D(x_0, 2.5) = 11$, and the defect ratio is therefore $DR(x_0, 2.5) = 11/21 = 0.52$. (C) Defect ratio $DR(x_0, r)$ plotted against $A(x_0, r)$ for increasing radii r centered around the target voxel. Plotted as a vertical line is $A(x_0, 2.5)$ and as an area plot the corresponding value of $DR(x_0, 2.5)$ from Figure 2B). The horizontal line indicates the threshold parameter T = 0.5. (D) Cluster score $C(x_0, r)$ plotted against normalized area $N(x_0, r)$. The cluster score $C(x_0, r)$ corresponds to the values of $DR(x_0, r)$ greater than the threshold T, scaled from 0 to 100. $N(x_0, r)$ is obtained by dividing $A(x_0, r)$ by A_{lung}. The $DDI(x_i)$ is obtained by calculating the area plotted in red (see Equation 1). (D) The DDI output map showing the $DDI(x_i)$ for all defect voxels. The value for our target voxel is $DDI(x_0) = 28$. The mean DDI per defect voxel for this lung map is DDI = 11.6. DDI, defect distribution index

$$T = 0.5$$

$$N(x_i, r) := \frac{|A(x_i, r)|}{A_{lung}}.$$

T is a parameter that defines a minimum defect ratio required for a collection of voxels to be considered a cluster. It could theoretically be any number between 0 and 1. Values closer to 0 tend to capture more loosely connected defects as single clusters. Values close to 1 lead to defect clusters being identified only if they contain no healthy voxels, which makes the algorithm more sensitive to noise. Here, voxels are considered to be part of a cluster if their surroundings are made up of more defect voxels than non-defect voxels. T was therefore chosen to be 0.5. More information on the rationale for using parameter T and its effects can be found in the Supporting Information and Supporting Information Figure S2, available online.

Defect voxels that are surrounded by defect at a density greater than the minimum defect ratio T therefore have a positive cluster score $C(x_i, r)$. The cluster score for any given circle centered around the target voxel is 100 if it is completely made up of defect voxels, and 0 if the defect ratio is exactly equal to T.

Defect voxels, which are part of a denser or more extended defect cluster, have an increased and positive value of $C(x_i, r)$ for the same value of r compared to defect voxels in less dense or less extended clusters (Figure 3).

Values for the normalized area are expressed as multiples of the lung area approximation A_{lung}. A value of $N(x_i, r) = 1$ corresponds to a circle whose value of $A(x_i, r)$ is the same as the area of the lung. Note that values of $N(x_i, r)$ can go beyond 1 because circles of radius r can contain non-lung background voxels and be larger than the lung. Including non-lung background voxels in the calculation of the defect ratio ensures that identical clusters of defect accumulate the same DDI when they are located at the edge of the lung as in the center of a lung slice.

3. Finally, we perform a stepwise integration of the discrete values of cluster score $C(x_i, r)$ as a function normalized area $N(x_i, r)$ as we increase the value of r. We continue to increase r as long as $C(x_i, r)$ remains positive.

For the set of increasing radii $r_0, r_1, \ldots, r_n$ with distinct associated values of $A(x_i, r)$, where r_n is the largest radius with a positive value of $C(x_i, r)$, we define the DDI as follows:

$$DDI(x_i) := \sum_{k=1}^{n} C(x_i, r_k) \cdot (N(x_i, r_k) - N(x_i, r_{k-1})).$$

To obtain the outcomes on the slice and patient level, it is now possible to calculate the mean of the $DDI(x_i)$ across any subset of defect voxels, whether that is all defect voxels across the k slices (for a patient level outcome) or a subregion of 1 slice

(Figure 2E). The use of a shared normalization by A_{lung} across the k slices of the same lung ensures that defect clusters of identical size and shape receive the same DDI within the same lung, regardless of the size of the slice they are located in.

2.1 | Example of DDI on artificial lung images

The DDI is illustrated for different exemplary patterns of defect distributions (homogeneously scattered, multiple smaller clustered defects, 1 clustered defect) with the exact same extent of DP of 25% in Figure 4. The DDI is most sensitive for large round-shaped clustered defects. The DDI assesses to what extent each defect voxel in the defect map is located in the middle of a defect cluster. This results in increasing DDI for clustered defects, as well as for increasing DP. Further examples of DDI are presented in the Supporting Information Figure S3, available online.

3 | METHODS

3.1 | Study design

This methodological study used MRI data that was previously obtained in a single-center, cross-sectional, observational study between March 2016 and January 2019 at the University Children's Hospital of Bern (Bern, Switzerland).[20,21]

3.2 | Study population

Data of 53 pediatric CF patients were included. Eligibility criteria were 1) a confirmed CF diagnosis, 2) the ability to perform MRI and pulmonary function tests, and 3) no requirements for supplementary oxygen. Study participants successively underwent nitrogen multiple breath washout, spirometry, body plethysmography, and MRI measurements during 1 visit. Functional MRI scans were followed by morphological MRI scans from which the Eichinger score was derived as an overall marker of disease severity.[25] Informed consent was provided by parents, or by participants if they were older than 14 years of age. Ethical approval was obtained for this study (EKNZ 2015-326 and KEK 2017-00279), and some of the data were published before.[20,21] More detailed descriptions on functional and morphological MRI and pulmonary function tests can be found here as well.

3.3 | MRI data acquisition

Subjects underwent MRI measurements without sedation using a 1.5 Tesla whole body MRI scanner (Magnetom
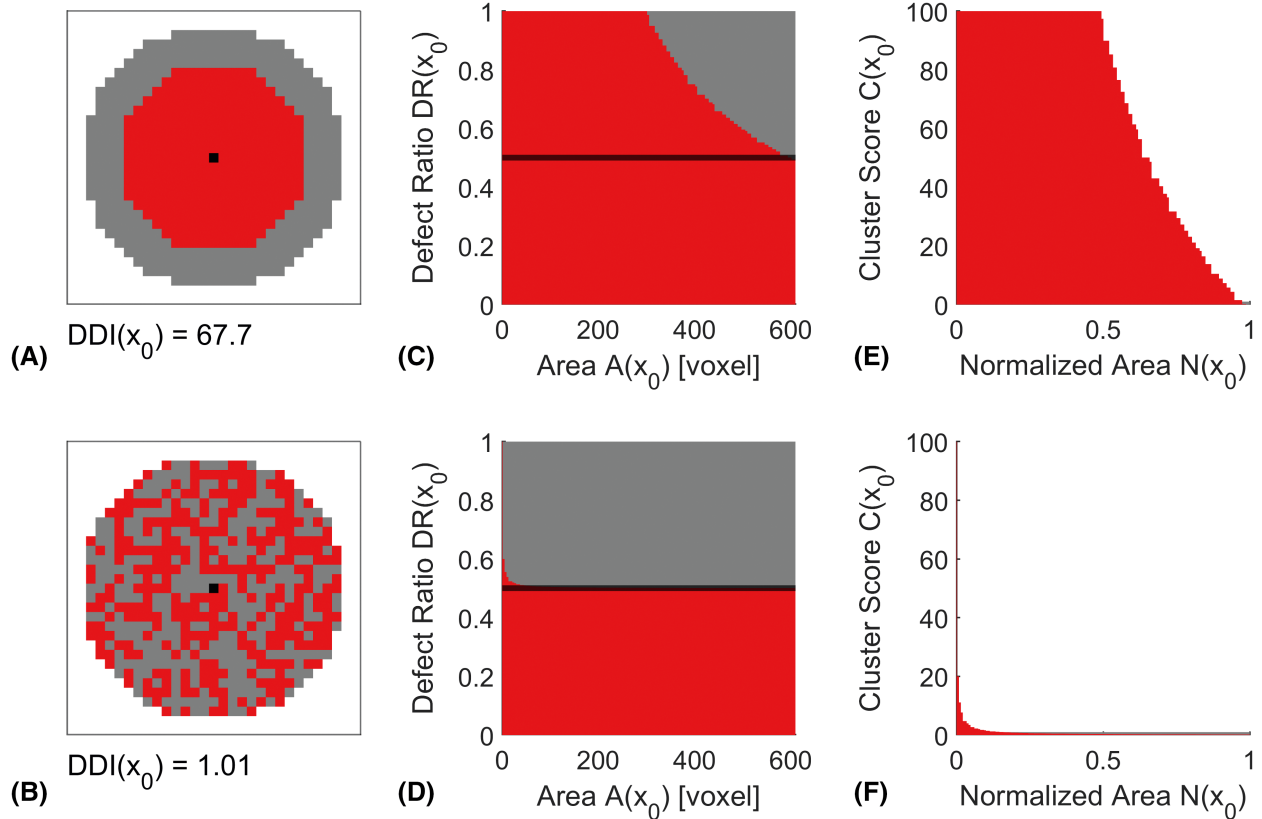
FIGURE 3 $DDI(x_i)$ depends on the surrounding defect distribution. The maps shown in (A) and (B) contain the same number of defect voxels (red) and the same number of non-defect voxels (gray). The calculation for the central voxel in black is shown. (A) Target voxel in black is surrounded by defect voxels (red) in a solid cluster. (B) Target voxel is surrounded by a scattered defect distribution. In this case, each new annulus is occupied by the same number of defect- and non-defect voxels. (C) and (D): The target defect voxels have an identical number of defect voxels present in the same map but different values of defect ratio for circles of any given area centered around the target voxel. (E) and (F) This results in different cluster scores and therefore different $DDI(x_0)$ outputs
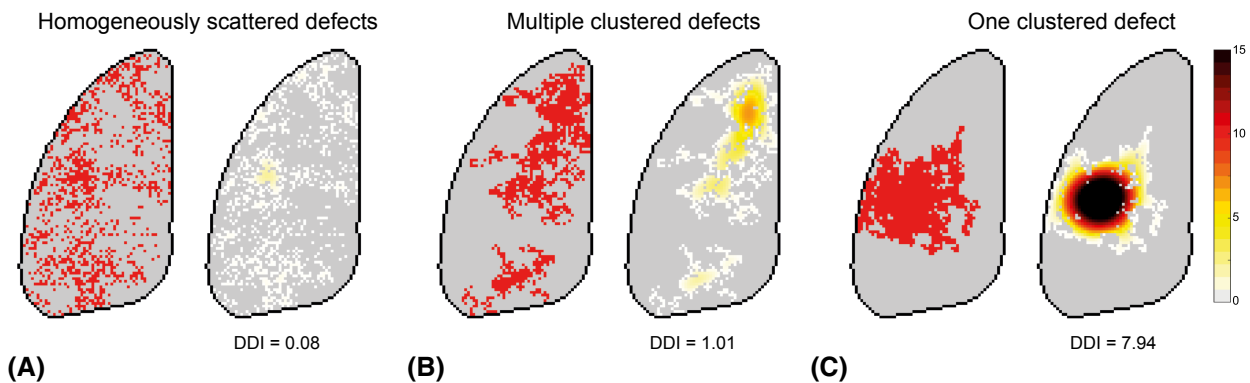
FIGURE 4 DDI applied to artificial lung defect maps with different defect distributions. (A) Homogeneously scattered defect. (B) Multiple smaller clustered defects. (C) One clustered defect. Left image: artificial lung defect map with DP = 25%. Defect voxels are labeled in red, non-defect lung voxels in gray. Right image: corresponding visualization of the DDI, darker colors indicate higher DDI per defect voxel (range = 0-15). DP, defect percentage

Aera; Siemens Healthineers, Erlangen, Germany) with a 12-channel thorax and a 24-channel spine receiver coil array. An ultrafast steady-state free precession pulse sequence[26] was used to obtain time-resolved 2D image series of the lungs. Images were acquired at 6-11 coronal slice positions to cover the whole lung. Pulse sequence parameters were as follows: FOV = 450 × 450 mm^2, matrix size = 128 × 128, TE/TR = 0.67/1.46 ms, flip angle = 60°, slice thickness = 12 mm, bandwidth = 2056 Hz/voxel, acquisition time per image = 110 ms, acquisition rate = 3.3 images/s, acquisition time

per slice = 48 s, GRAPPA factor = 2, and predefined default shim settings (tune-up).

3.4 | Functional imaging and defect quantification

An algorithm that aligns lung structures while maintaining ventilation and perfusion signal modulations[27] was applied to register the 2D image time series to an image in the midrespiratory state (baseline image). Subsequently, fractional ventilation and relative perfusion maps were obtained from the registered time-series using the MP method (Figure 1A,B).[19]
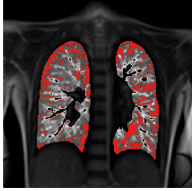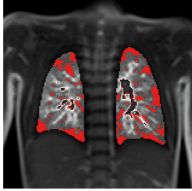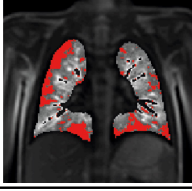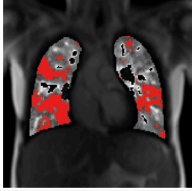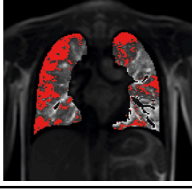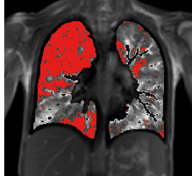
Automatic segmentation with vessel exclusion was performed on the baseline images using an artificial neural network as previously described,[28] after which the DP was determined.[20,29] The DP equals the number of defect lung voxels divided by the number of lung area voxels for each slice. All voxels below 70% of the median value of the signal intensity histogram were defined as defect, resulting in a binary lung defect map. Per participant, R_{FV} and R_Q were calculated by dividing the total number of defect voxels by the total number of lung area voxels of all the slices for ventilation and perfusion, respectively (Figure 1C,D).[20]

3.5 | The visual scoring system

A visual scoring system that describes the presence of clustered defects within a functional lung defect map was developed prior to developing the DDI. The score ranges from 1 (scattered distribution of defects) to 6 (1 clustered defect) (Figure 5). The MP MRI defect maps of the study population, 395 perfusion- and thereafter 395 ventilation-defect slices, were rated independently by 3 different raters. Raters had, respectively, 6 (R1), 12 (R2), and 24 (R3) months of experience with MP MRI data. R1 scored the defect slices twice (24 h apart). Mean visual scores of 3 raters were reported on the level of individual slices. On the patient level, a weighted arithmetic mean based on the slice size was calculated from the mean visual scores of the individual slices. This was done to ensure a proportional contribution of each slice to the patient level visual score, preventing uneven contributions of small anterior or posterior slices.

3.6 | The defect distribution index

The DDI algorithm was applied to the MP MRI defect maps of the study population. On the slice level, DDI output maps were created, and the mean DDI was calculated. On the patient level, the mean DDI over all slices was calculated.

Visual Score	Criteria	Defect map example
1	Defects are homogeneously scattered over full lung. No or hardly any clusters.	
2	Defects are relatively homogeneously scattered. Very small defect clusters.	
3	No homogeneously scattered defect distribution. Small defect clusters.	
4	Defects are relatively homogeneously scattered. Very small defect clusters.	
5	Multiple larger defects, but few non-defect voxels can be recognized within. Some smaller defects migh be present.	
6	One or two large defects cluster with hardly any non-defect voxels within the defect cluster. No, or hardly any, other affected lung regions.	

FIGURE 5 Visual scoring system describing the defect distribution for MP MRI defect maps with examples for score 1 to 6. For each visual score, an image example is displayed

3.7 | Statistical analysis

Study population characteristics were expressed as median (interquartile range) values. Spearman's rank correlation coefficients (r) were reported for all correlations because data distributions were skewed according to Shapiro-Wilk tests and visual inspection. P values $< .05$ were considered statistically significant. For multiple comparisons, a Bonferroni correction was applied. The intraclass correlation coefficient (ICC) was calculated to assess intra- and interrater agreement

of the visual scoring system. Based on the ICCs and their corresponding 95% confidence intervals (CI), agreement is defined as moderate (0.40-0.59), good (0.60-0.79), or very good (>0.80).[30] Analyses were reported for ventilation and perfusion separately.

First, agreement between the new index and human perception of defect distributions was determined on the slice level. The visual scoring was carried out on the slice level, and the mean of 3 raters was compared to the slice level mean of the DDI. To create a patient level mean of the visual scoring, visual scores of slices were weighted by their size. This weighted arithmetic mean score was then compared to the mean of the DDI across all the slices of a patient. Additionally, correlations between the DDI on the patient level, and the DP, lung clearance index (LCI in turnovers), forced expiratory volume in 1 s, forced expiratory flow 25%-75%, and Eichinger score were calculated.

MatLab version 2019b (MathWorks, Natrick, MA) and Stata version 16.0 (StataCorp, College Station, TX) were used.

4 | RESULTS

4.1 | Study population

The main study population characteristics can be found in Table 1. MRI measurements were performed successfully in all 53 CF patients. LCI data were missing for 9 study participants because ≥ 2 quality-controlled measurements could not be obtained. Spirometry data were missing for 3 different participants. Calculation of DDI was feasible for all MRI data. The mean calculation time per patient (ventilation and perfusion together) is 3.2 s (SD = 3.3 s). The median DDI is 1.77 (1.35 to 2.68) and 1.32 (0.87 to 2.60) for ventilation- and perfusion-defect maps, respectively.

4.2 | Defect distribution index versus visual scoring system

Intrarater agreement for the visual scoring system is very good, with an ICC of 0.88 (95% CI: 0.84-0.91) for ventilation- and 0.88 (95% CI: 0.85-0.90) for perfusion-weighted defect maps. Interrater agreement is good (ICC = 0.75 (95% CI: 0.72-0.79) for ventilation; ICC = 0.74 (95% CI: 0.70-0.77) for perfusion). All P values are < .001.

Strong correlations between the DDI and the mean visual score are found on the slice and the patient level for both ventilation ($r = 0.90$ on slice level; $r = 0.89$ on patient level) and perfusion ($r = 0.88$ on slice level, $r = 0.91$ on patient level) with P values < .0001 (Figure 6). Examples

TABLE 1 Study population characteristics. Median (interquartile range) [range] is reported

CF patients (N = 53)			
Age (years)	11.9	(9.1 to 14.7)	[6.1 to 17.8]
Gender (*n*, males/ females)	19/34		
LCI (TO) (*n* = 44)	9.9	(8.2 to 12.4)	[6.5 to 17.6]
FEV_1 (z-scores) (*n* = 50)	−1.0	(−2.1 to −0.3)	[−5.5 to 1.8]
$FEF_{25\%-75\%}$ (z-scores) (*n* = 50)	−1.2	(−2.3 to 0.1)	[−4.7 to 1.6]
Eichinger score (*n* = 53)	5	(2 to 10)	[0 to 22]
Defect percentage			
R_{FV} (%)	25.9	(19.3 to 28.1)	[9.9 to 35.9]
R_Q (%)	23.0	(18.5 to 25.6)	[11.8 to 31.4]
Defect distribution index			
DDI ventilation	1.7	(1.3 to 2.7)	[0.5 to 6.4]
DDI perfusion	1.3	(0.9 to 2.6)	[0.4 to 4.1]
Visual image score[1]			
Ventilation	3.4	(2.9 to 3.9)	[1.5 to 5.3]
Perfusion	3.2	(2.6 to 3.7)	[1.7 to 4.8]

CF, cystic fibrosis; DDI, defect distribution index; $FEF_{25\%-75\%}$, forced expiratory flow 25%-75%; FEV_1, forced expiratory volume in 1 s; LCI, lung clearance index; TO, lung volume turnovers; R_{FV}, impaired fractional ventilation; R_Q, impaired relative perfusion.

[1]Mean visual score, patient.

of MP MRI defect maps with similar DPs but different defect distributions (and thus visual scores), as well as the corresponding DDI outcomes, are shown in Figure 7. As can be seen in the images, the DDI distinguishes between more scattered and more clustered defect distributions over a different range of DPs.

4.3 | Lung function parameters

Correlations between the DDI, DP, lung function parameters, and the CF structural disease score are provided in Table 2 and are shown as scatter plots in the Supporting Information Figure S4. DDI correlates moderately to strongly with the DP ($r = 0.61$ for ventilation; $r = 0.75$ for perfusion) (Figure 8). Moderate correlations are found with the LCI ($r = 0.48$ for ventilation; $r = 0.55$ for perfusion), and Eichinger score ($r = 0.51$ for ventilation; $r = 0.54$ for perfusion). Correlations with spirometry outcome measures are weak and not statistically significant for ventilation defect maps.

5 | DISCUSSION

5.1 | Main findings

The DDI quantifies the defect distribution in functional lung MRI. The DDI distinguishes scattered from clustered defects and is applicable to MP MRI lung data of a large CF population. This new index shows very good agreement with a newly developed visual scoring system, resembling human perception of defect distributions. Correlations between the DDI and well-established lung function parameters indicate that the DDI is complementary to currently reported outcomes.

5.2 | Comparison with previous studies

There are various methods to describe the defect distribution in lung MRI. A straightforward method is describing the defects by anatomical regions, such as lung lobes. However, lobar lung segmentation in MRI is challenging and currently not widely available. A study in adults showed that it may be possible, using a CT-based lung lobe library; however, the authors themselves conclude that the results should be better interpreted as an estimate, and the method is computationally very intensive.[23,31] Several research groups addressed this by geometrically subdividing the lungs.[17,29,32,33] Although allowing for defect localization, it does not describe the defect distribution as an entity itself and thereby differs from the DDI.

The largest defect and number of defects were determined from hyperpolarized gas MRI in CF patients.[24] Those measures give an estimation of the defect distribution as well. In general, the DDI is higher for large defects and lower in case of multiple (smaller) defects. However, the largest defect and number of defects reflect only 1 single image component each. The DDI, on the other hand, makes use of all
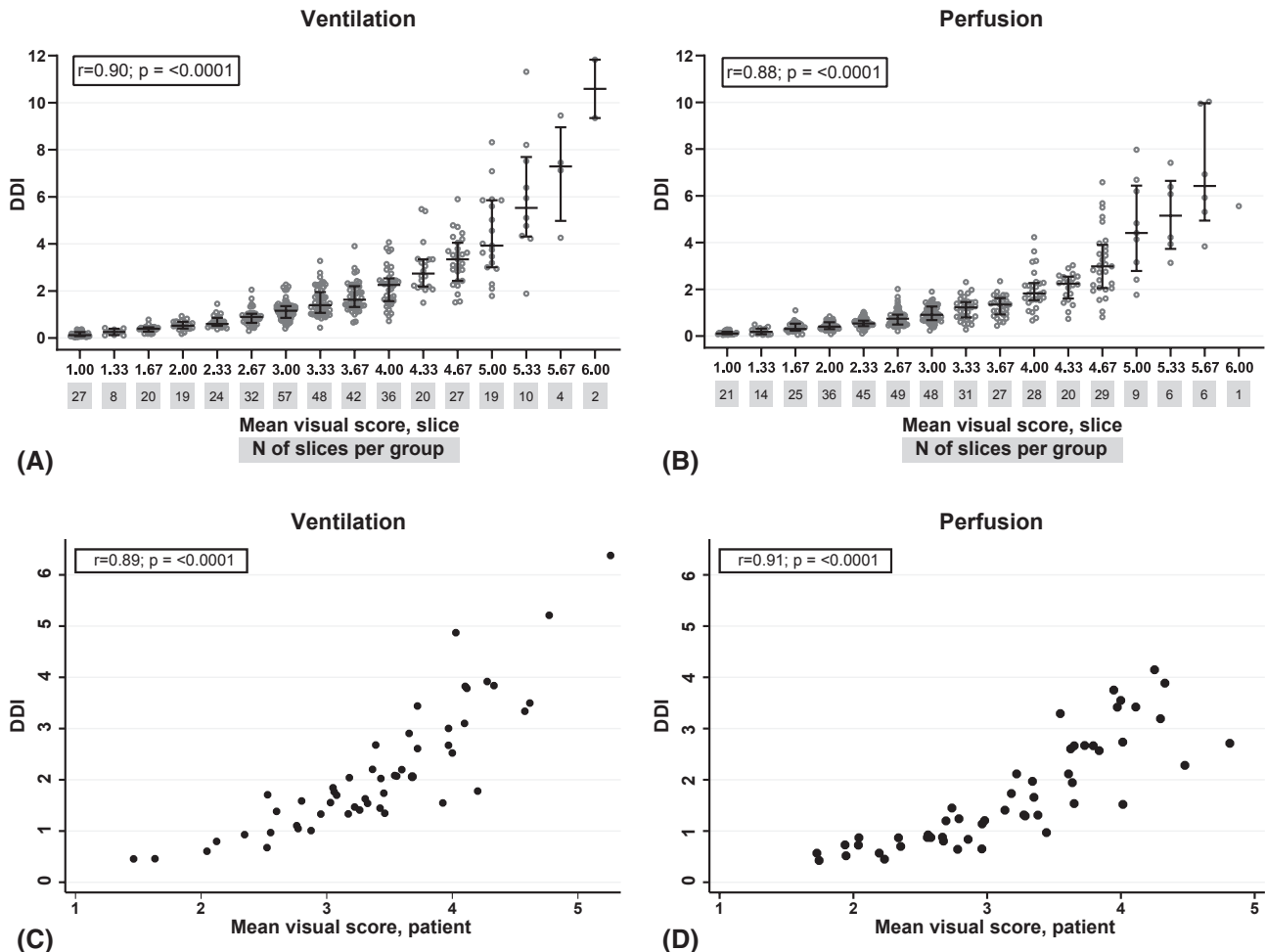
FIGURE 6 DDI versus visual scoring system for (A) ventilation and (B) perfusion MP MRI slices and for (C) ventilation and (D) perfusion patient-level outcomes. In (A) and (B), the data is grouped per visual score, where gray circles represent individual slices and solid lines represent the median and the interquartile range. As an additional x-axis, the exact number of slices per visual score is given on gray background. The upper left box in each graph represents the Spearman rank correlation coefficient and corresponding *P* value. *P* values < .05 are considered statistically significant
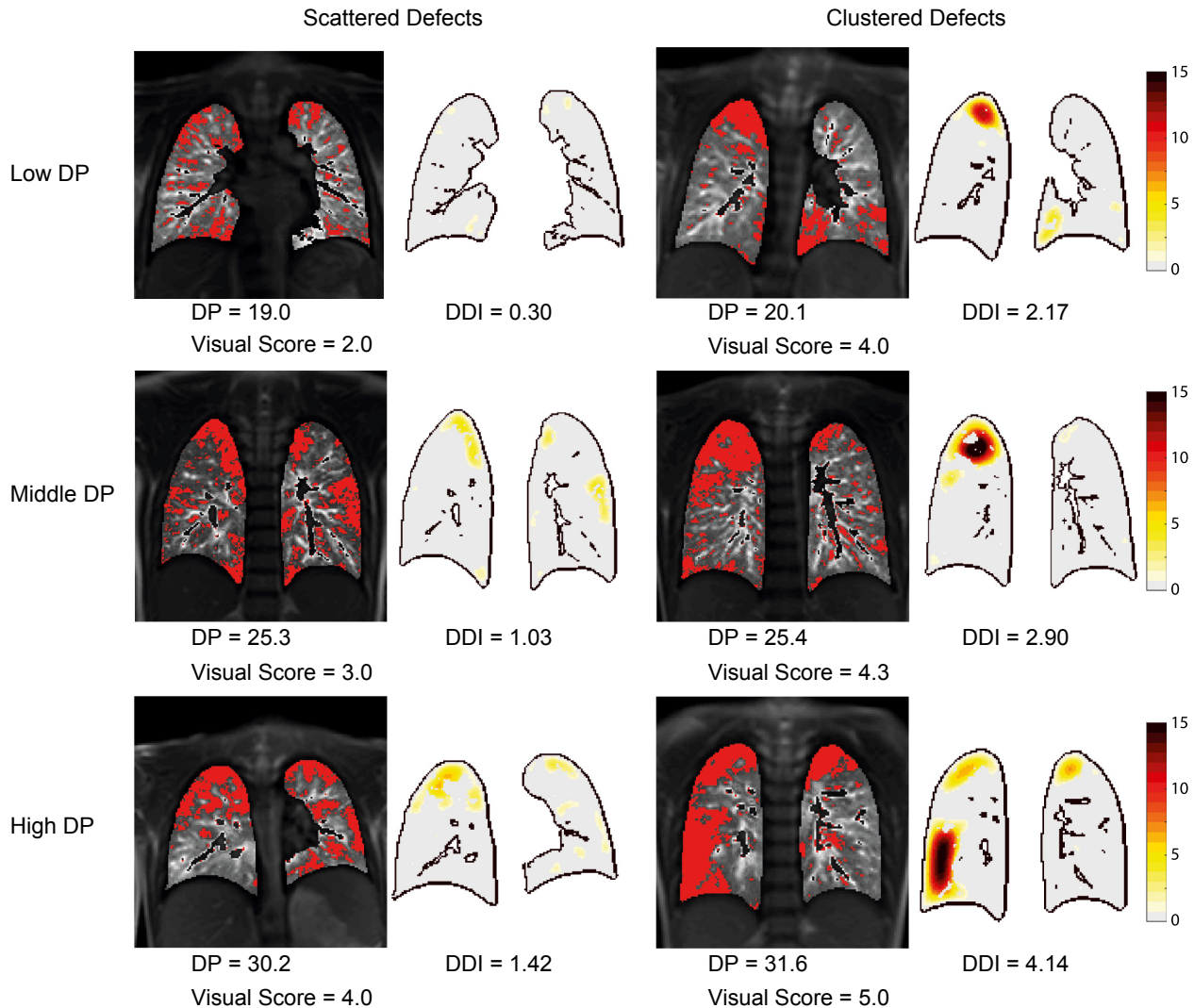
FIGURE 7 DDI applied to exemplary MP MRI perfusion defect maps of CF patients with different defect distributions (columns) over a range of defect percentage (rows). Left image = perfusion-weighted MP MRI defect map. Right image = corresponding visualization of the DDI; darker colors indicate higher DDI per defect voxel (color range = 0-15). Top left: LCI = 6.5 TO; FEV_1 = −0.44 z-scores. Top right: LCI = 10.1 TO; FEV_1 = 0.52 z-scores. Mid-left: LCI = n/a; FEV_1 = −1.40 z-scores. Mid-right: LCI = n/a; FEV_1 = −0.36 z-scores. Bottom left: LCI = 12.7 TO; FEV_1 = −1.86 z-scores. Bottom right: LCI = 14.7 TO; FEV_1 = −1.50 z-scores

information present within the image. It reflects the overall density of all the defects within the lung. As an illustration, the largest defect and number of defects would be the same for a lung image with 1) 2 large defects; and 2) 1 large and 1 relatively small defect. The DDI could distinguish between both situations, giving a higher score to the lung image with 2 large clustered defects.

5.3 | Strengths and limitations

A strength of this research is that we developed a metric that assesses a new aspect of the defect image than the currently reported DP does. Not only defect size but also defect distribution are now quantified, and more spatial information is gained from functional defect maps. The interpretation of the

DDI is rather intuitive. It has a minimum value that approximates 0, which corresponds to a scattered defect distribution. The more the defects are clustered, the higher the DDI becomes. Another strength of the DDI is that it is applicable to any binary lung mask. The use of the DDI is not limited to MP MRI but is generalizable to any quantitative MRI technique from which lung defect maps are obtained.

In addition, the DDI is tested in a large dataset of CF patients. These data were previously obtained from a study in which adherence to the study protocol was always warranted and standardized equipment was used.[20,21] The index is validated against a visual scoring system, confirming its potential to quantify the defect distribution in accordance with human perception. The visual scores correlate strongly with the DDI on the slice and patient levels. The DDI is scalable and thereby independent of lung size. This makes it suitable

for longitudinal analysis and interindividual comparison of defect distributions.

It should be noted that the visual scoring system seems to be dependent on the DP. Relatively large clustered defects are more likely to be recognized as clusters by the human eye than relatively small clustered defects. In agreement with this human perception of defect distributions, the DDI depends on the DP as well. The DDI is designed to quantify large clustered defects; we had hypothesized that large clustered defects are more clinically relevant than small ones. This makes the DDI inherently dependent on the DP. One could argue that this decreases the additional value of the DDI to the DP. However, DDI values differ for lung images with similar DPs but different defect distributions. This shows that, although being correlated, the DP and DDI still reflect different aspects of the same images.

TABLE 2 Overview of correlation coefficients between the DDI and lung function parameters and cystic fibrosis structural disease score (Eichinger score)

	DDI ventilation		DDI perfusion	
	r	P value	r	P value
DP (%) (n = 53)	0.61	< .0001[a]	0.75	< .0001[a]
LCI (TO) (n = 44)	0.48	.0011[a]	0.55	.0001[a]
FEV$_1$ (z-scores) (n = 50)	−0.24	.14	−0.49	.0007[a]
FEF$_{25\%-75\%}$ (z-scores) (n = 50)	−0.31	.026	−0.47	.0005[a]
Eichinger Score (n = 53)	0.51	.0001[a]	0.54	< .0001[a]

r = Spearman's rank correlation coefficient; DP = defect percentage (R$_{FV}$ for ventilation; R$_Q$ for perfusion).

[a]A Bonferroni correction is applied, and P values < .005 (0.05/10) are considered statistically significant.
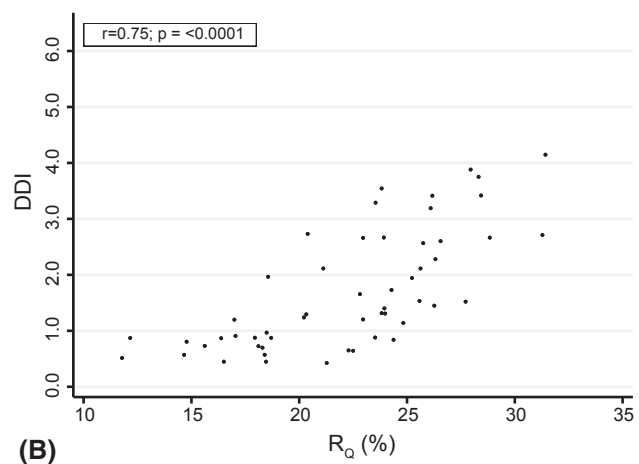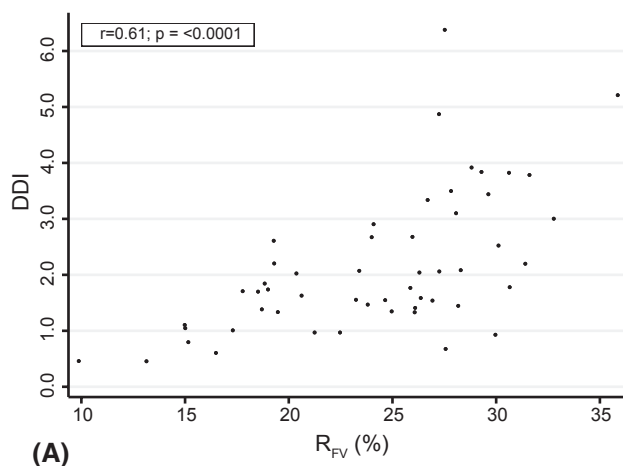
Because the DDI depends on the DP, it inherently also depends on the chosen defect quantification method. In the current work, the DDI was applied to defect maps for which the method of defect quantification was previously validated.[29] In theory, the DDI is applicable to defect maps obtained using any method of defect quantification.

5.4 | Clinical relevance and next steps

From the correlations between the DDI and existing lung function parameters, it can be concluded that the DDI assesses a different aspect of lung impairment. The DP quantifies defect size, whereas the DDI assesses defect distribution. The LCI is a measure of overall ventilation inhomogeneity, which can be insensitive to nonventilated regions and such a situation can be hypothesized in the case presented in Figure 1B.[34,35] The DDI, on the other hand, is extremely sensitive for clustered defect regions. The DDI is calculated from functional lung imaging, which was proven to detect lung disease already in an early stage.[36] In contrast, FEV1 is nowadays reported in advanced lung disease[37,38] and therefore not associated strongly to DDI. The DDI is thus complementary to existing lung function parameters. Reporting the DDI next to those parameters provides additional information on lung disease.

5.5 | Outlook

The DDI allows for observer-independent intra- and interindividual comparison of defect distributions. Because this is a methodological study, we would suggest applying the DDI in a clinical research setting to investigate how differences in defect distributions affect clinical outcomes. It seems worthwhile to investigate the complementary information of the DDI as outcome measure in addition to other outcome measures of

FIGURE 8 Correlation between the DDI and the DP (R$_{FV}$ for ventilation; R$_Q$ for perfusion) for (A) ventilation and (B) perfusion MP MRI data of 53 CF patients. Correlation coefficients are statistically significant. R$_{FV}$, impaired fractional ventilation; R$_Q$, impaired relative perfusion

lung disease in CF such as LCI or DP. Further, effectiveness of inhaled drugs, for example, antibiotics in patients with CF, depends on regional lung function.[39-41] Quantifying the distribution of functional lung defects may give insight in whether inhalation therapy might be beneficial for specific patients, which would allow for personalized treatment.

The DDI is currently applied to 2D MRI data. It could be adapted for 3D as well by using spheres instead of rings for identification of voxels that contribute to the DDI. Application of the DDI to 3D data assesses the whole lung situation more closely and may provide even more insight in lung disease.

6 | CONCLUSION

The DDI is a novel index for functional lung MRI defect maps, describing another aspect of the images than the currently reported defect percentage. It allows for quantification of defect distributions, which at the moment is only qualitatively described by radiologists. It is applicable to MP MRI data, as shown for a large pediatric CF population.

ORCID
Anne Valk https://orcid.org/0000-0002-6190-0438
Corin Willers https://orcid.org/0000-0003-1140-9437
Orso Pusterla https://orcid.org/0000-0003-1879-055X
Grzegorz Bauman https://orcid.org/0000-0001-6972-0776
Florian Wyler https://orcid.org/0000-0002-1232-1392
Philipp Latzin https://orcid.org/0000-0002-5239-1571

REFERENCES
1. Elborn JS. Cystic fibrosis. *Lancet*. 2016;388:2519-2531.
2. Ratjen F, Bell SC, Rowe SM, et al. Cystic fibrosis. *Nat Rev Dis Primers*. 2015;1:15010.
3. Mott LS, Park J, Murray CP, et al. Progression of early structural lung disease in young children with cystic fibrosis assessed using CT. *Thorax*. 2012;67:509-516.
4. Stick SM, Brennan S, Murray C, et al. Bronchiectasis in infants and preschool children diagnosed with cystic fibrosis after newborn screening. *J Pediatr*. 2009;155:623-628.e1.
5. Kołodziej M, de Veer MJ, Cholewa M, Egan GF, Thompson BR. Lung function imaging methods in cystic fibrosis pulmonary disease. *Respir Res*. 2017;18:96.
6. Kuo W, Ciet P, Tiddens HAWM, et al. Monitoring cystic fibrosis lung disease by computed tomography. Radiation risk in perspective. *Am J Respir Crit Care Med*. 2014;189:1328-1336.
7. Pearce MS, Salotti JA, Little MP, et al. Radiation exposure from CT scans in childhood and subsequent risk of leukaemia and brain tumours: a retrospective cohort study. *Lancet*. 2012;380:499-505.
8. Ferris H, Twomey M, Moloney F, et al. Computed tomography dose optimisation in cystic fibrosis: a review. *World J Radiol*. 2016;8:331-341.
9. Owens CM, Aurora P, Stanojevic S, et al. Lung clearance index and HRCT are complementary markers of lung abnormalities in young children with CF. *Thorax*. 2011;66:481-488.
10. Ramsey KA, Rosenow T, Turkovic L, et al. Lung clearance index and structural lung disease on computed tomography in early cystic fibrosis. *Am J Respir Crit Care Med*. 2016;193:60-67.
11. Thomen RP, Walkup LL, Roach DJ, et al. Hyperpolarized (129) Xe for investigation of mild cystic fibrosis lung disease in pediatric patients. *J Cyst Fibros*. 2017;16:275-282.
12. Gutberlet M, Kaireit TF, Voskrebenzev A, et al. Repeatability of regional lung ventilation quantification using fluorinated ((19)F) gas magnetic resonance imaging. *Acad Radiol*. 2019;26:395-403.
13. Goralski JL, Chung SH, Glass TM. Dynamic perfluorinated gas MRI reveals abnormal ventilation despite normal FEV1 in cystic fibrosis. *JCI Insight*. 2020;5. http://dx.doi.org/10.1172/jci.insight.133400.
14. Stahl M, Wielpütz MO, Graeber SY. Comparison of lung clearance index and magnetic resonance imaging for assessment of lung disease in children with cystic fibrosis. *Am J Respir Crit Care Med*. 2016. http://dx.doi.org/10.1164/rccm.201604-0893oc.
15. Bauman G, Puderbach M, Deimling M, et al. Non-contrast-enhanced perfusion and ventilation assessment of the human lung by means of Fourier decomposition in proton MRI. *Magn Reson Med*. 2009;62:656-664.
16. Kjørstad Å, Corteville DMR, Henzler T, et al. Quantitative lung ventilation using Fourier decomposition MRI; comparison and initial study. *MAGMA*. 2014;27:467-476.
17. Veldhoen S, Weng AM, Knapp J, et al. Self-gated non-contrast-enhanced functional lung MR imaging for quantitative ventilation assessment in patients with cystic fibrosis. *Radiology*. 2017;283:242-251.
18. Voskrebenzev A, Gutberlet M, Klimeš F, et al. Feasibility of quantitative regional ventilation and perfusion mapping with phase-resolved functional lung (PREFUL) MRI in healthy volunteers and COPD, CTEPH, and CF patients. *Magn Reson Med*. 2018;79:2306-2314.
19. Bauman G, Bieri O. Matrix pencil decomposition of time-resolved proton MRI for robust and improved assessment of pulmonary ventilation and perfusion. *Magn Reson Med*. 2017;77:336-342.
20. Nyilas S, Bauman G, Sommer G. Novel magnetic resonance technique for functional imaging of cystic fibrosis lung disease. *Eur Respir J*. 2017;50:1701464. http://dx.doi.org/10.1183/13993003.01464-2017.
21. Nyilas S, Bauman G, Pusterla O, et al. Ventilation and perfusion assessed by functional MRI in children with CF: reproducibility in comparison to lung function. *J Cyst Fibros*. 2019;18:543-550.
22. Washko GR, Parraga G. COPD biomarkers and phenotypes: opportunities for better outcomes with precision imaging. *Eur Respir J*. 2018;52:1801570. http://dx.doi.org/10.1183/13993003.01570-2018.

23. Tustison NJ, Qing K, Wang C, Altes TA, Mugler JP 3rd. Atlas-based estimation of lung and lobar anatomy in proton MRI. *Magn Reson Med*. 2016;76:315-320.

24. Smith LJ, Collier GJ, Marshall H. Patterns of regional lung physiology in cystic fibrosis using ventilation magnetic resonance imaging and multiple-breath washout. *Eur Respir J*. 2018;52:1800821. http://dx.doi.org/10.1183/13993003.00821-2018.

25. Eichinger M, Optazaite D-E, Kopp-Schneider A, et al. Morphologic and functional scoring of cystic fibrosis lung disease using MRI. *Eur J Radiol*. 2012;81:1321-1329.

26. Bauman G, Pusterla O, Bieri O. Ultra-fast steady-state free precession pulse sequence for Fourier decomposition pulmonary MRI. *Magn Reson Med*. 2016;75:1647-1653.

27. Sandkühler R, Jud C, Pezold S, Cattin PC. *Adaptive Graph Diffusion Regularisation for Discontinuity Preserving Image Registration*. Cham, Switzerland: Springer International Publishing; 2018. https://doi.org/10.1007/978-3-319-92258-4_3.

28. Willers C, Bauman G, Andermatt S. The impact of segmentation on whole-lung functional MRI quantification: repeatability and reproducibility from multiple human observers and an artificial neural network. *Magn Reson Med*. 2021;85:1079-1092.

29. Bauman G, Puderbach M, Heimann T, et al. Validation of Fourier decomposition MRI with dynamic contrast-enhanced MRI using visual and automated scoring of pulmonary perfusion in young cystic fibrosis patients. *Eur J Radiol*. 2013;82:2371-2377.

30. Portney LG, Watkins MP. *Foundations of Clinical Research: Application to Practice*. Norwalk, CT: Appleton & Lange; 1993.

31. Qing K, Tustison NJ, Mugler JP, et al. Probing changes in lung physiology in COPD using CT, perfusion MRI, and hyperpolarized Xenon-129 MRI. *Acad Radiol*. 2019;26:326-334.

32. Kohlmann P, Strehlow J, Jobst B, et al. Automatic lung segmentation method for MRI-based lung perfusion studies of patients with chronic obstructive pulmonary disease. *Int J Comput Assist Radiol Surg*. 2015;10:403-417.

33. Tustison NJ, Altes TA, Song G, et al. Feature analysis of hyperpolarized helium-3 pulmonary MRI: a study of asthmatics versus nonasthmatics. *Magn Reson Med*. 2010;63:1448-1455.

34. Horsley AR, Davies JC, Gray RD, et al. Changes in physiological, functional and structural markers of cystic fibrosis lung disease with treatment of a pulmonary exacerbation. *Thorax*. 2013;68:532-539.

35. Robinson PD, Cooper P, Van Asperen P, Fitzgerald D, Selvadurai H. Using index of ventilation to assess response to treatment for acute pulmonary exacerbation in children with cystic fibrosis. *Pediatr Pulmonol*. 2009;44:733-742.

36. Wielpütz MO, Puderbach M, Kopp-Schneider A, et al. Magnetic resonance imaging detects changes in structure and perfusion, and response to therapy in early cystic fibrosis lung disease. *Am J Respir Crit Care Med*. 2014;189:956-965.

37. de Jong PA, Nakano Y, Lequin MH, et al. Progressive damage on high resolution computed tomography despite stable lung function in cystic fibrosis. *Eur Respir J*. 2004;23:93-97.

38. Tiddens HAWM, Puderbach M, Venegas JG, et al. Novel outcome measures for clinical trials in cystic fibrosis. *Pediatr Pulmonol*. 2015;50:302-315.

39. Dubsky S, Fouras A. Imaging regional lung function: a critical tool for developing inhaled antimicrobial therapies. *Adv Drug Deliv Rev*. 2015;85:100-109.

40. Dubsky S, Fouras A. The role of functional lung imaging in improvement of pulmonary drug delivery. In: Nokhodchi A, Martin GP, eds. *Pulmonary Drug Delivery: Advances and Challenges*. Chichester, UK: Wiley-Blackwell; 2015.

41. Tiddens HA, Bos AC, Mouton JW, Devadason S, Janssens HM. Inhaled antibiotics: dry or wet? *Eur Respir J*. 2014;44:1308-1318.

SUPPORTING INFORMATION

Additional Supporting Information may be found online in the Supporting Information section.

FIGURE S1 Scalability of DDI. Normalizing the DDI by the lung area (ie, number of lung voxels), makes the DDI scalable. As presented in the figure, lung images with the same defect pattern (1 circular cluster, 25% defect), but different numbers of lung voxels (ie, either sizes or resolutions), receive the same DDI. DDI: Defect Distribution Index

FIGURE S2 Effects of varying values of parameter T and varying amount of defect, as a hypothetical result of different defect quantification approaches. From left to right the value of parameter T increases, resulting in a decrease in DDI. From bottom to top, the amount of defect increases, resulting in an increase in DDI

FIGURE S3 DDI and defect shape. A) Artificially created defect maps (Lung area = 4000 voxels; DP = 20%) showing 1) round-, 2) square-, 2) rectangle-, and 4) serpentine-shaped defects. B) Corresponding visualization of the DDI; darker colors indicate higher DDI per defect voxel (range = 0-15). The DDI algorithm calculates a DDI using a variable circle size. In addition, defect voxels in proximity of the target voxel contribute more to the DDI than defect voxels that are further away. Therefore, the DDI is most sensitive for round-shaped clustered defects. DDI: Defect Distribution Index

FIGURE S4 Scatter plots of the DDI with lung function parameters and cystic fibrosis structural disease score (Eichinger score). Scatter plots for LCI are shown in A) and B), for FEV1 in C) and D), for FEF25-75% in E) and F) and for Eichinger score in G) and H). r: Spearman's rank correlation coefficient (A Bonferroni correction is applied and P-values < 0.005 (0.05/10) are considered statistically significant, see Table 2 in the main manuscript); LCI: lung clearance index; TO: lung volume turnovers; FEV1: forced expiratory volume in 1 second; FEF25-75%: forced expiratory flow 25-75%